

Title	Fully porous GaN p-n junctions fabricated by chemical vapor deposition: a green technology towards more efficient LEDs
Authors	Carvajal, Joan J.;Mena, Josue;Bilousov, Oleksandr V.;Martínez, Oscar;Jiménez, Juan J.;Zubialevich, Vitaly Z.;Parbrook, Peter J.;Geaney, Hugh;O'Dwyer, Colm;Diaz, Francesc;Aguilo, Magdalena
Publication date	2015-05
Original Citation	Carvajal, J. J., Mena, J., Bilousov, O., Martínez, O., Jiménez, J., Zubialevich, V. Z., Parbrook, P. J., Geaney, H., O'Dwyer, C., Díaz, F. and Aguiló, M. (2015) '(Invited) Fully Porous GaN p-n Junctions Fabricated by Chemical Vapor Deposition: A Green Technology towards More Efficient LEDs', ECS Transactions, 66(1), pp. 163-176. doi: 10.1149/06601.0163ecst
Type of publication	Article (peer-reviewed)
Link to publisher's version	http://ecst.ecsdl.org/content/66/1/163.abstract - 10.1149/06601.0163ecst
Rights	© 2015 ECS - The Electrochemical Society
Download date	2024-04-26 03:55:39
Item downloaded from	https://hdl.handle.net/10468/6692

Fully porous GaN *p-n* junctions fabricated by Chemical Vapor Deposition: a green technology towards more efficient LEDs

J. J. Carvajal^a, J. Mena^a, O. V. Bilousov^a, O. Martínez^b, J. Jiménez^b, V.Z. Zubialevich^c, P.J. Parbrook^{c,d}, H. Geaney^{c,e}, C.O'Dwyer^{c,e}, F. Díaz^a and M. Aguiló^a

^a Física i Cristal·lografia de Materials i Nanomaterials (FiCMA-FiCNA) and EMaS, Universitat Rovira i Virgili (URV), Marcel·lí Domingo, 1, E-43007, Spain

^b GdS-Optronlab, Departamento de Física Materia Condensada, Univ. de Valladolid, Edificio I+D, Paseo de Belén, 11, 47011, Valladolid, Spain

^c Tyndall National Institute, Lee Maltings, Dyke Parade, Cork, Ireland

^d School of Engineering, University College Cork, Cork, Ireland

^e Department of Chemistry, University College Cork, Cork, Ireland

Porous GaN based LEDs produced by corrosion etching techniques have demonstrated enhanced light extraction efficiencies in the past. However, these fabrication techniques require further post-growth processing steps, which increase the price of the final device. In this paper, we review the process we developed for the formation of fully porous GaN *p-n* junctions directly during growth, using a sequential chemical vapor deposition (CVD) process to produce the different layers that form the *p-n* junction.

Introduction

The discovery of light-emitting porous Si (1) propelled investigations of porosity formation in semiconductors (2-4). Porous semiconductors have received considerable interest, primarily due to their unusual optical and electrical properties, that sometimes can be radically different from those of the bulk material. Here we should consider not only basic semiconductor parameters like conductivity, band gap energy and absorption/emission of light, which might be quite different, but also internal symmetries/anisotropies, high-order effects and even basic chemistry. Some of the novel properties discovered for porous semiconductors are: (i) fast chemical reactions practically not previously observed in bulk materials, including violent explosions due to the large surface to volume ratio and optical diffusion conditions (5); (ii) novel absorption characteristics (e.g., transparency for UV while blocking longer wavelengths (6)); (iii) optical anisotropy (7) and new types of optical anisotropy not encountered in natural materials if two or more sets of pores are present simultaneously (8); (iv) strongly decreased thermal conductivity (and concomitantly changed phonon spectra) (9); (v) strongly changed the electrical conductivity, sensitive to the presence of gases or humidity (10); among others.

The recent advances in the production technologies of porous semiconductor materials together with the unique properties that these materials exhibit have promoted the utilization of them in the fabrication of devices for advanced nanoelectronics, sensors with enhanced sensitivity, interfacial structures and catalysis (11). The actual applications

of these materials, however, depend on the development of processing methods able to precisely control the optical and electrical properties of the resulting porous materials.

Among porous semiconductor materials, wide band gap semiconductors, and in particular porous GaN, play an important role in developing new technologies for applications in optoelectronics, magnetism, catalysis and biotechnology.

GaN is considered to be one of the most important semiconductors nowadays for a number of applications in electronics and optoelectronics, principally due to its wide direct band gap (3.39 eV at room temperature) (12). The large band gap of GaN, coupled with its thermal stability and excellent physical properties, make it an excellent candidate for high temperature electronics (13). GaN also has a high heat capacity and thermal conductivity (14-16) making it suitable for high power and high frequency applications. Furthermore, GaN can withstand ionizing radiations better than other semiconductor materials, which makes GaN a good option for space, betavoltaics and photovoltaics use (17-18). GaN crystallizes in the hexagonal system with the space group $P6_3mc$ (wurtzite structure) (19). GaN-based laser diodes are used to read blue-ray discs while GaN high-electron-mobility transistors (HEMTs) are used in various wireless infrastructures. GaN-based metal-oxide-semiconductor and metal-semiconductor field-effect transistors (MOSFET and MESFET, respectively) offer many advantages in high power electronics for automotive applications. However, the most important application of GaN is found in light emitting diodes (LEDs) as the active light emitting element of various optical components, ranging from traffic lights to large area displays.

In its porous form, GaN has received particular interest in the last decade due to interesting optical and electronic properties that allowed, for instance, the demonstration of gas sensors with enhanced sensitivity and also LEDs with improved light extraction efficiency, of crucial importance for the modern society, since a significant amount of energy consumed is used for lighting. Porous GaN exhibits some interesting specific properties. A strong photoresponse was observed in epitaxial GaN layers grown on 6H-SiC substrates and anodized in aqueous solutions of HF (20). It has been proved that porous GaN exhibited lesser stress compared to its bulk counterpart (21). In some cases it has been observed that porous GaN shifts its band edge emission further into the UV due to quantum confinement that appears due to wire-like structures in porous GaN (22). Finally, it has been reported that photoluminescence (PL) intensity in porous GaN increases with respect to its bulk counterpart (23).

Porous GaN has typically been fabricated by (photo)electrochemical etching and chemical etching methods. For instance, porous GaN has been produced by anodic etching (24) using a 0.1 M NaOH solution with 0.2 M NaCl, a Pt electrode as cathode and GaN as anode, and a DC voltage supply that provided constant current between the electrodes through the NaOH electrolyte. This process led to formation of pores over the whole area of the GaN film after the etching process. Porous GaN has also been produced by Pt-assisted electroless etching (25). The process did not require any external voltage or electrical contact to the sample, with etching initiated by simply immersing a Pt-coated GaN substrate in a solution of methanol, HF and hydrogen peroxide in a 1:2:1 volume ratio, and illuminating it with a mercury lamp to enhance the process. In that case, the morphology was dominated by the formation of ridge structures that evolved over etching time, with a deep porous network in between and under the ridges. UV-assisted photoelectrochemical wet etching has also been used to produce porous GaN (23,26) using a buffered HF aqueous solution ($\text{HF}:\text{H}_2\text{O} = 2:1$, volume ratio) as electrolyte, a Pt electrode as cathode and GaN as anode. Another way of producing porous GaN has been through alternating current, photo-assisted electrochemical etching (22) in a 4 wt % KOH

electrolyte under UV illumination and with a 50 Hz sine-wave AC current, using a Pt and GaN as cathode and anode, respectively. This technique allowed the formation of well-defined layers of hexagonal like pores of GaN with sizes that increased with etching time, and that depended on the quality of the starting GaN epilayers.

However, the outlined (electro)chemical reactions are sensitive to many parameters, such as the electrolyte chemistry, applied potential or current density, temperature, electrolyte flow conditions, doping type and doping concentration of the semiconductor, illumination, and surface conditions (i.e. polished, rough, masked). These limitations, together with the complex equipment required to control each parameter, and the fact that many electrolytes are highly toxic and/or corrosive, makes the production process challenging from a technical point of view.

Despite all these limitations, porous GaN has been used in a wide range of applications. For instance, porous GaN thin films have been used as buffer layers in growing epitaxial GaN layers with a lower level of defects (28), or in a lift-off process of GaN and devices through an electrochemical anodization process to generate a voided region with decreased lateral fracture resistance (29). Porous GaN has also been used to fabricate Schottky diode gas sensors for hydrogen detection with high sensitivity (30-31). Porosity in GaN has also been used to enhance the light extraction and internal quantum efficiencies of GaN-based LEDs (32-40).

Given the wide ranging possible applications of porous GaN, it is worthy to explore new production techniques for porous GaN that overcome the limitations listed above, and if possible, simplify the synthetic processes. In this context, we have been able to produce porous GaN through the direct reaction of metallic Ga with NH_3 in a simple chemical vapor deposition (CVD) system that does not require any secondary electrochemical or electroless etching or subsequent chemical treatment after growth to induce the porosity (41,42). This approach is simpler and cheaper than pre-existing technologies. Also, it does not use corrosive electrolytes or toxic metallorganic compounds, allowing for the generation of a green technology for the production of porous GaN. This technique allowed us to produce micrometer sized nanoporous GaN particles on BN substrates (41) and to deposit porous GaN directly onto Si substrates in a single growth step (42). Furthermore, by using Mg_3N_2 as Mg-precursor, *p*-type porous GaN could be produced using the same technique (43), and if the concentration is high enough, MgO-GaN metal-oxide-semiconductor (MOS) diodes could be fabricated in a single deposition step (44). This motivated us to investigate the possibility of developing new electronic and optoelectronic devices with improved external quantum efficiencies, the incorporation of phosphors for LEDs, and high surface area sensing.

Here we report a summary of the most important achievements obtained in this field, namely the epitaxial growth of *n*-type and *p*-type porous GaN thin films on non-porous GaN substrates to fabricate functional porous GaN *p-n* junctions.

Results and Discussion

Influence of the substrate on the texturation of porous GaN films

Different substrates were investigated to ascertain if they might play a role in the crystallographic orientation of porous GaN particles. In a first attempt we used amorphous SiO_2 (fused silica), tungsten wire, (111) silicon, and pyrolytic boron nitride (p-BN), as substrates. We have chosen these substrates with the criterion of using an amorphous substrate (fused silica), a cubic substrate different than Si and without a

particular crystallographic orientation (W wire), and a substrate with hexagonal structure (p-BN). We also tested (111) Si since it has been reported that (0001) GaN films can be deposited on these substrates (45). Since this is the direction along which the pores of GaN are aligned (46), it can provide a way to orient the porous GaN particles. In all cases, with the exception of (111) Si, we sprayed an ethanolic solution of $\text{Ni}(\text{NO}_3)_2$ on the surface of the substrates to facilitate the nucleation of GaN. (111) Si substrates were coated with 20 nm thick films of Au, Pt, Ti or W, used as catalysts for the growth of porous GaN.

To grow these porous particles, gallium metal (99.99%) and ammonia (>99.98%) were used as the Ga and N sources, respectively. The reactor was degassed to a vacuum pressure of 1×10^{-2} Torr, after which NH_3 was introduced through a mass-flow controller at a flow rate of 75 sccm and the furnace heated to 1203 K, while the pressure was kept at 15 Torr. The reaction was continued at this temperature and pressure for 60 min under a constant flow of NH_3 . Growth was halted by cooling to room temperature without NH_3 flow.

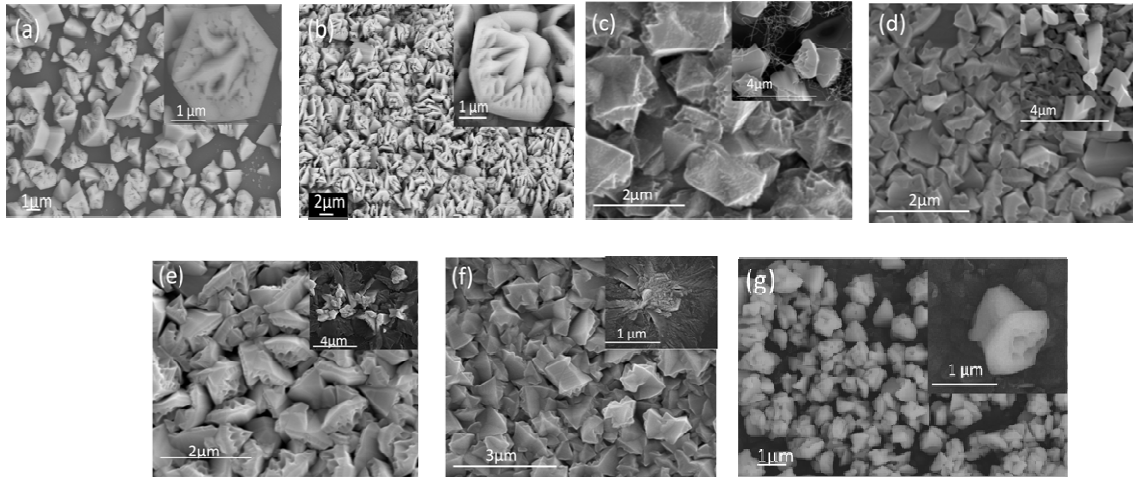


Figure 1. SEM images of the nanoporous GaN particles grown on different substrates: (a) amorphous SiO_2 (fused silica), (b) W wire, (c-f) (111) Si coated with different catalysts (c) Au, (d) Pt, (e) Ti and (f) W and (g) pyrolitic BN.

SEM pictures of the nanoporous GaN particles grown on these substrates reveal in all cases that GaN appears in the form of hexagonal micron-sized nanoporous particles (see Figure 1). When using fused silica, the level of porosity in the particles is low, with the pores more concentrated at the central part of the particles, and with an elongated shape towards the external parts of the particles (see Figure 1(a)). On the W wire, the density of micron-sized nanoporous particles is very high (see Figure 1(b)). Meanwhile, GaN grown on (111) Si substrates coated with different catalyst appears in the form of micron-sized nanoporous particles with a mean particle size of 2-5 μm (see Figures 1 (c-f)). The lowest level of porosity was obtained when W was used as catalyst (see Figure 1 (f)). In most of the cases, nanowires were also observed together with the porous particles, especially when Au and Pt were used as catalysts (see insets in Figures 1 (c-d)). When Ti and W were used as catalysts, apparently an early stage of epitaxial growth is observed at the edges of the samples (see insets in Figures 1 (e-f)), but it fades away in the center of the sample where a higher density of particles is observed. According to these images it

seems that the combination of the substrate and the catalyst play a relevant role in the morphology of the particles. Finally, in the case of p-BN, a certain degree of alignment of the GaN particles can be observed, since a bigger number of pores perpendicular to the surface can be seen (see Figure 1 (g)); however, due to the misalignment of the BN flakes that form the p-BN substrate, there are also particles with different crystallographic orientations. Also the degree of porosity in these particles is lower than in the other cases.

XRD characterization of these samples, as expected from the SEM pictures, did not reveal any preferential growth along any particular direction, with the exception of those grown on a (111) Si substrate coated with Ti and W. This might be related to the fact that the interlayer formed by the catalyst, and located between the substrate and the GaN layer, hampers the influence that the structure of the substrate has on the growing GaN layer. In the case of the porous layers grown on (111) Si substrates coated with Ti and W, XRD characterization reveals an incipient degree of texturation of the films, as confirmed by the non-uniform distribution of the intensity in the Debye rings observed with the GADDS detector (see Figure 2) and the different intensity of the diffraction peaks when compared to the reference XRD pattern for GaN (00-050-0792 JCPDS file) included in Figure 2 (c) for comparison. This is more evident when we compare this XRD pattern with any of those recorded for the porous GaN particles obtained using other catalysts. The results for a (111) Si substrate coated with $\text{Ni}(\text{NO}_3)_2$ are included in the figure to visualize this effect. However, from the data obtained, it is not an easy task to determine what the preferential orientation of the particles is, since the decrease in intensity is observed for diffraction peaks with components in all crystallographic directions. A closer look to the intensity of the peaks seems to indicate that those that have a component along the c crystallographic direction tend to decrease in intensity, which would indicate that the preferential orientation of the particles is perpendicular to this direction. In fact, the peak that preserved its expected intensity is that corresponding to the $(11\ \bar{2}0)$ plane, which would indicate that the preferential orientation should be along the $[11\ \bar{2}0]$ direction or combination of components in the a and b crystallographic directions. However, we could not record other diffraction peaks of the family of planes to confirm this hypothesis.

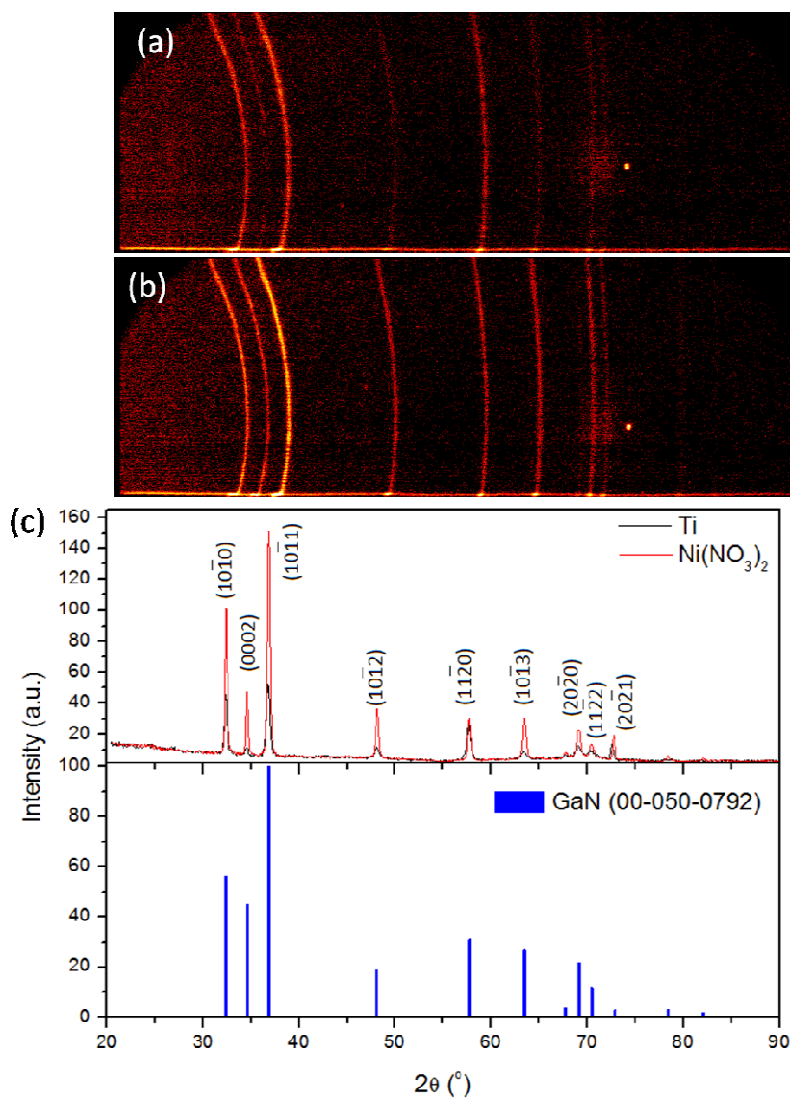


Figure 2. X-ray diffraction patterns of nanoporous GaN obtained on (111) Si substrates coated with Ti and Ni(NO₃)₂. (a,b) Debye rings recorded for both samples, respectively, and (c) diffraction patterns. The reference pattern of GaN from JCPDS (00-050-0792) has been included for comparison.

Chemical Vapor Deposition on patterned (111) Si substrates

This incipient texturation observed in some of the samples obtained on (111) substrates coated with Ti and W, encouraged us to follow this idea of crystallographically orienting the porous GaN particles by using patterned (111) Si substrates coated with Ti to reduce the number of nanoporous GaN particles that nucleate on the surface of the substrate. We decided to choose Ti as catalyst since previous studies have shown that it can act as a pre-orienting layer for deposition of GaN on glass substrates for LEDs applications, since Ti crystallizes also in the hexagonal system with a relative small lattice mismatch with GaN ($\Delta a/a = 7.4\%$) (47).

To do that, as the base material we used commercial (111) Si wafers coated with a thermally grown SiO₂ thin layer, 50 nm thick (MicroChemicals). The SiO₂ layer was patterned with a 2D array of holes, 1.5 μm in diameter, using laser lithography and

etching techniques. Metallic Ti was deposited inside the holes by sputtering. To create the microhole patterning on SiO₂, the wafer was initially heated at 473 K for 10 min to remove any moisture present on the surface of the wafer. Then, the wafer was coated with ~700 nm layer of AZ 1505 photoresist (MicroChemicals) by spin coating, and softbaked at 373 K for 30 s. The photoresist was illuminated with a 405 nm laser to create the pattern of holes in an area of 1 cm² using the laser lithography system, according to the design previously established in the computer controlling the system. A buffered HF solution was used as the chemical agent to remove the SiO₂ layer of the substrate in the areas not protected by the photoresist. After that, and before the remaining photoresist was removed, we coated the surface of the wafer with a 20 nm thick sputtered Ti layer. In this way we coated the exposed surface of Si with a Ti layer that acts as the metallic catalyst for the growth process of porous GaN. Finally, the photoresist was removed from the surface by using a resist stripper solution. Together with the photoresist, the Ti layer deposited on the top of the photoresist was removed, while that covering the bottom of the holes and deposited on Si remained. Figure 3 summarizes the patterning process.

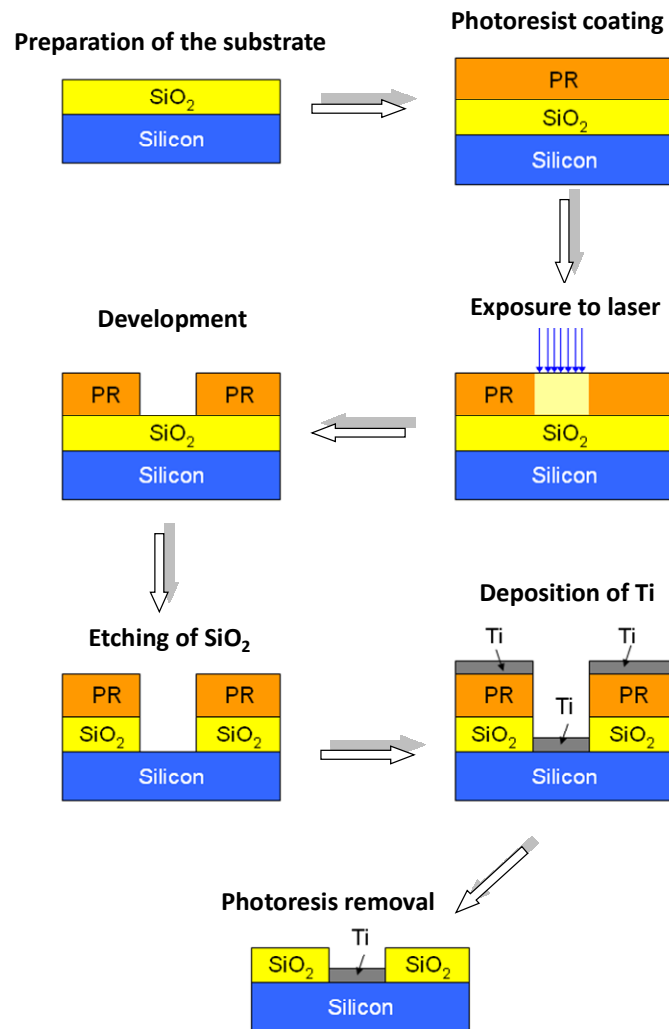


Figure 3. Scheme of the process of patterning of SiO₂ on (111) Si wafers with a 2D array of holes, 1.5 μm in diameter.

Figure 4 shows SEM images of the patterned SiO₂ on (111) Si wafers. In the image recorded with secondary electrons (see Figure 4 (a)) we can observe the array of holes, with diameters ranging from 1.4 to 1.5 μm, with a separation between holes of 2 μm, both in vertical and horizontal directions. In the image recorded with backscattered electrons (see Figure 4 (b)) we can observe that Ti, appearing with a lighter color in the image, is located only inside the holes.

These patterned substrates were coated with nanoporous GaN particles, by introducing them in the CVD system, and reducing the reaction time to 15 min to avoid overgrowth of porous GaN microparticles. As can be seen in Figure 4 (c), a well-ordered structure was obtained, covering the whole area of the patterned substrate. The growth was restricted to the patterned area which coincides with the Ti-seeded regions. However, porous GaN was grown in the form of aggregated micron-sized nanoporous GaN particles without any preferential crystallographic orientation, as can be seen in the inset in Figure 4 (c). The XRD pattern, shown in Figure 4 (d), indicates that it does not exhibit any preferential growth direction for this sample, as confirmed by the homogeneous distribution of intensity in the Debye rings (see inset in Figure 4(d)).

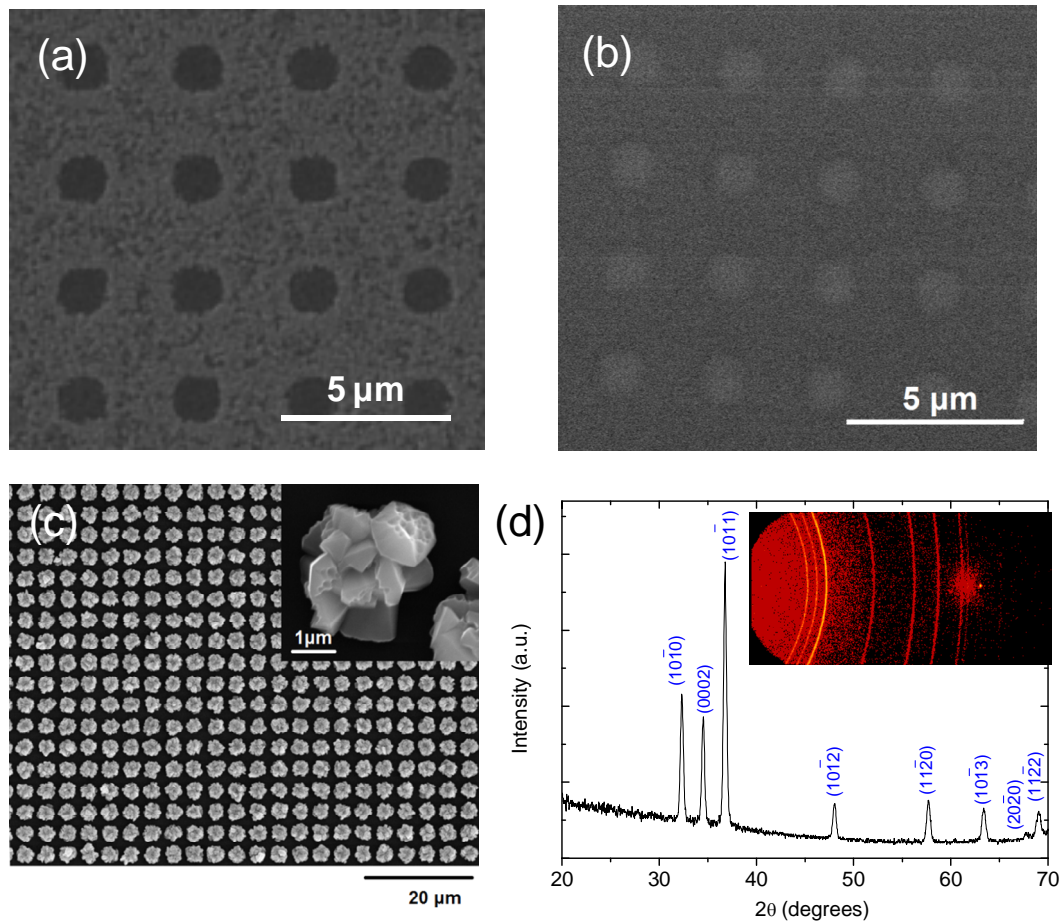


Figure 4. SEM images of the patterned SiO₂ on (111) Si substrate recorded using (a) secondary electrons and (b) backscattered electrons. (c) SEM image of the ordered porous GaN structure grown by CVD on the patterned substrates with inset showing a higher magnification image. (d) XRD pattern recorded for this structure with the corresponding Debye rings (inset).

To understand the lack of any preferential growth in this case, we performed additional experiments by reducing the reaction times to 5, 10 and 12 min. The results are shown in Figure 5. As can be seen from the images, at early stages, the crystal growth process starts from the edges of the microholes and progresses towards the center of the microhole. Thus, the crystallographic orientation of the GaN particles, expected through an orientational effect of the metallic catalyst, is missed due to the nucleation of the GaN particles on the SiO₂ walls of the holes which have an amorphous structure.

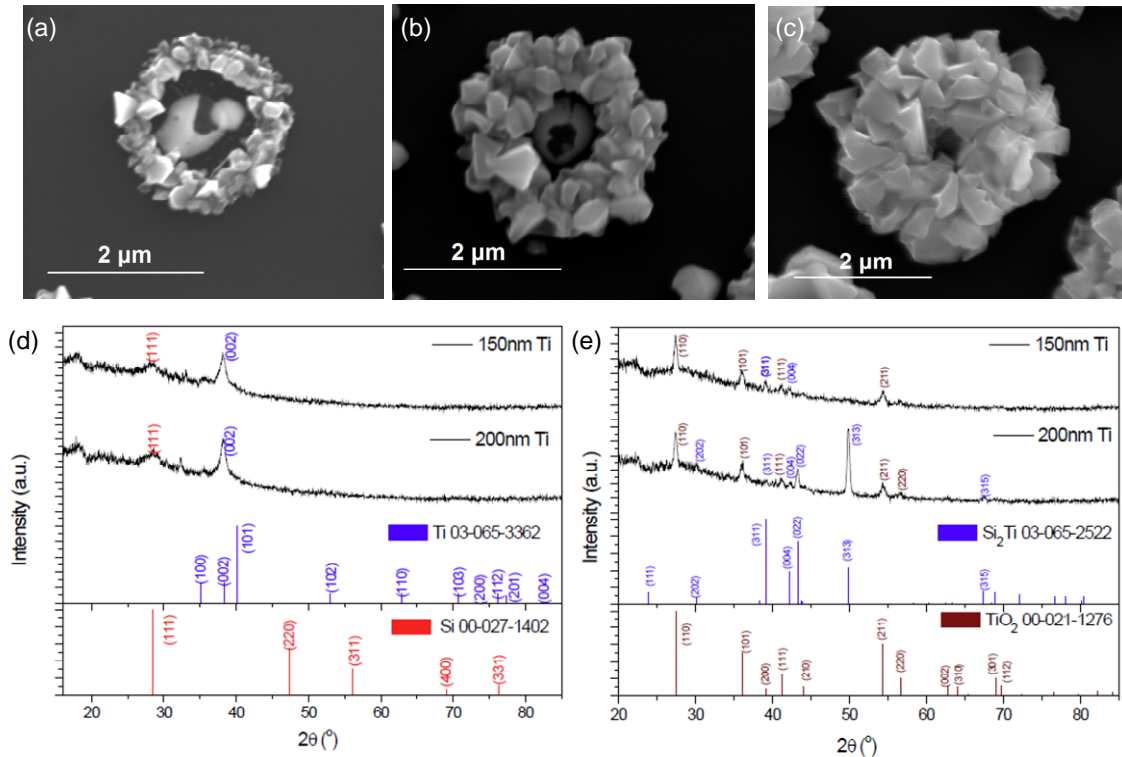


Figure 5. SEM images of porous GaN on patterned SiO₂ on (111) Si substrates at different growth stages (a) 5, (b) 10 and (c) 12 min. (d) XRD patterns of the SiO₂ on (111) Si substrates coated with a Ti thin film deposited by sputtering (d) as deposited and (e) after annealed in an NH₃ atmosphere replicating the reaction conditions for the deposition of porous GaN by CVD.

Particularly, the main reason hindering a crystallographic orientation of the porous GaN particles is the following. As deposited on (111)Si substrates Ti thin film is oriented along the [001] direction (see Figure 5 (d)). However, as seen from Figure 5(e), a conversion of metallic Ti to Si₂Ti alloy and to TiO₂ in its rutile form occurs when it is heated under conditions used for the growth of GaN, except the presence of metallic Ga. This indicates that Ti reacts with Si present both in the substrate and the SiO₂ coating layer to form the Si₂Ti alloy that has a different crystallographic structure (space group Fddd (03-065-2522 JCPDS file)); this process occurs likely in the central part of apertures. Also, in the edge regions of apertures Ti can react with the oxygen present on the SiO₂ coating layer to form rutile which crystallizes in the tetragonal system with space group P4₂/mnm (00-021-1276 JCPDS file).

Epitaxial growth of nanoporous GaN films

Finally, we decided to use a strategy in which no catalyst was used for the growth of GaN films. This entailed the removal of metallic catalysts and the use of substrates with a small lattice mismatch with GaN. Thus, *a priori*, the substrate which could provide the best results would be GaN itself, since it would provide a zero lattice mismatch with the porous layer. We investigated the possibility of obtaining an epitaxial porous layer by using a non-porous GaN thin layer grown on a sapphire substrate (48). Non-porous GaN substrates were grown on sapphire by metalorganic chemical vapor deposition using a standard process (49): high temperature sapphire wafer nitridation followed by a low temperature GaN nucleation and a high temperature coalescence step. Trimethylgallium and ammonia were used as precursors and hydrogen as a carrier gas. After growth of 3 μm thick nominally undoped GaN, disilane (Si_2H_6) was additionally introduced into the reactor chamber to deposit 1 μm thick top *n*-doped GaN:Si layer.

When growing porous GaN on the above described solid GaN templates, the optimum results were obtained for a deposition time of 30 min, since for longer times we observed that the pores tended to coalesce, forming elongated voids, while for shorter times, the thickness of the epitaxial layer was significantly reduced (48). Figure 6 (a) shows a SEM picture recorded at the surface of the porous layer, showing its porosity. The pores have typical diameters ranging from 200 to 300 nm, but more interestingly, the walls between pores have widths ranging from 10 to 50 nm. The rocking curve corresponding to the (0004) XRD reflection of the porous GaN epitaxial layer shows a FWHM of $1508''$, similar to that of the substrate ($1540''$), indicating the good structural quality of the epitaxial porous material obtained (see Figure 6 (b)). Also, a shift in the position of the rocking curve was observed which indicates a change in the strain condition of the porous material when compared to the substrate, which is apparently induced by ability to relax due to the internal porosity.

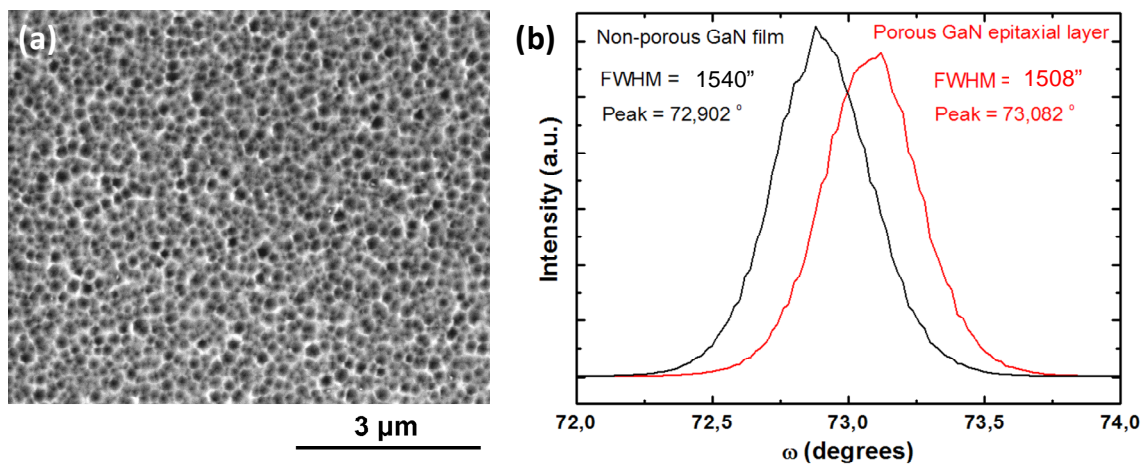


Figure 6. (a) Top view SEM image of a porous GaN epitaxial layer obtained on a non-porous GaN thin layer grown on a sapphire substrate. (b) Rocking curves of the (0004) reflection peak of the X-ray diffraction pattern recorded for the porous GaN epitaxial layer and the non-porous GaN substrate.

This growth approach allowed us to fabricate either partially or fully porous GaN diodes by CVD (50). Thus, *n*-type (48) or *p*-type (43) porous GaN epitaxial layers were

deposited on non-porous GaN substrates with complementary electrical conductivity to produce partially porous GaN diodes. To produce fully porous GaN diodes by CVD, a two step synthesis process was used in which first a *n*-type or *p*-type porous GaN epitaxial layer was produced, and then in the second step a new porous GaN epitaxial layer with complementary electrical conductivity was overgrown on the previous porous layer (50), as can be seen in the scheme shown in Figure 7 (a).

The electrical characterization of these structures confirms their diodic behavior, exhibiting the characteristic I-V curves with strong rectification, as can be seen in Figure 7(b). One interesting characteristics of these diodes is that the barrier to the exponential current increase is found to be in the range 0.5-0.68 V ($\sim(E_g/4q)-(E_g/2q)$) for the partially porous diodes, much lower than that expected in a non-porous GaN diode (E_g/q). This turn-on voltage is even lower in the fully porous *p-n* junctions, lying in the range $(E_g/4q) - (E_g/6q)$, resembling more the response observed in InN, GaN and other *p-n* junctions nanowires arrays (51,52). Microscopic characterization confirmed well-defined interfaces between the porous and the non-porous GaN (50), indicating that no significant tunneling barriers exist either at the GaN-GaN interface or on the surface of the GaN/Ohmic contacts. Thus, the barrier potentials are a function of the donor and acceptor densities. A second interesting characteristic is that the current at a fixed value for the forward voltage in the fully porous diodes is found to be three orders of magnitude higher than that measured in the partially porous diodes, which would result in a more efficient system from the electrical point of view. Electron beam induced current (EBIC) measurements (see Figure 7 (c)) indicate a homogeneous carrier recombination, since contrast was only observed for the bigger pores (the corresponding SEM image is also included in Figure 7 (c)). All these results demonstrate the good performance of the formed *p-n* junctions.

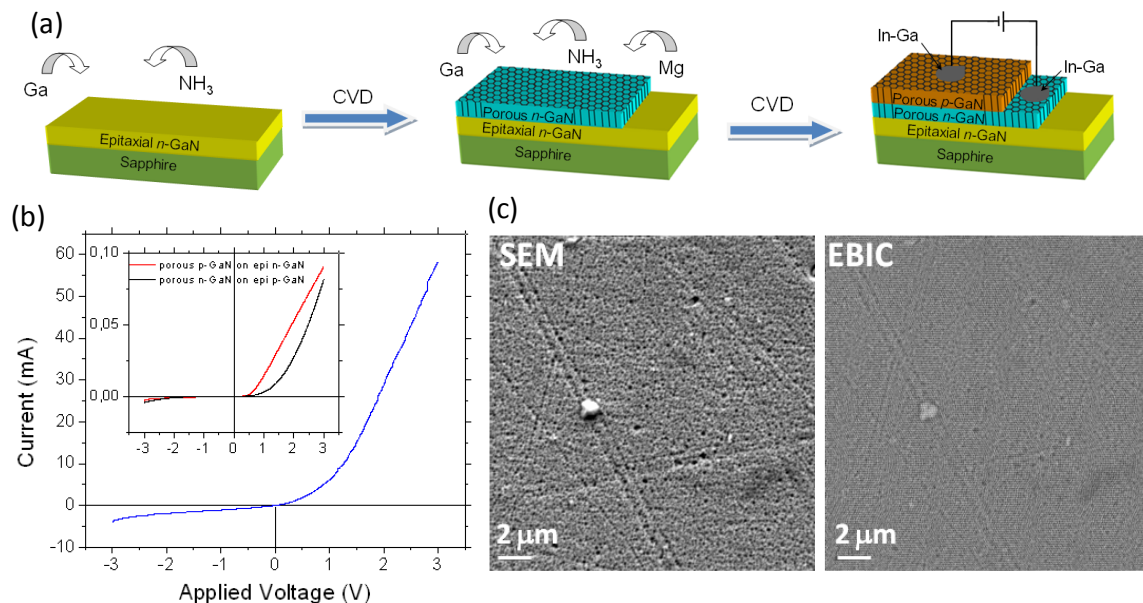


Figure 7. (a) Schematic representation of the fabrication process of fully porous GaN diodes by CVD. (b) I-V curves of the fully porous diode. Inset shows the I-V curves recorded for the partially porous diodes. (c) SEM and EBIC images of one of these diodes fabricated by CVD.

Conclusions

Taken as a whole, the investigation presented here demonstrates that partially and fully porous high quality GaN diodes can be fabricated by a CVD process, in which the lattice mismatch between the substrate and the porous GaN layer plays a crucial role, influencing both the degree of porosity and the crystallographic orientation of the porous GaN particles. We believe this investigation can be extended to other III-N materials such as InN and AlN to span the visible spectrum, and as a route towards porous, graded index III-N materials as a basis for white light LEDs incorporating other color centers, or for improving the light extraction and narrowing the output light cone for improved LED external quantum efficiencies. High surface area diodes produced by this route do not require complicated core-shell architectures in nanostructure arrays and may be viable routes to prepare chemically stable wide bandgap (bio)sensors.

Acknowledgments

This work has been supported by the Spanish Government under Projects No. MAT2011-29255-C02-02 and MAT2013-47395-C4-4-R, the Catalan Government under Project No. 2014SGR1358, and JCYL (VA293U13). F.D. acknowledges additional support through the ICREA Academia Award for Excellence in Research.

References

1. V. Lehmann, U. Gösele, *Appl. Phys. Lett.*, **58**, 856 (1991).
2. I.M. Tiginyanu, V.V. Ursaki, E. Monaico, E. Foca, H. Föll, *Electrochem. Solid-State Lett.*, **10**, D127 (2007).
3. C. O'Dwyer, D.N. Buckley, D. Sutton, M. Serantoni, S.B. Newcomb, *J. Electrochem. Soc.*, **154**, H78 (2007).
4. M.A. Steven-Kalceff, I.M. Tiginyanu, S. Langa, H. Föll, H.L. Hartnagel, *J. Appl. Phys.*, **89**, 2560 (2001).
5. D. Kovalev, V.Y. Timoshenko, N. Künzner, E. Gross, F. Koch, *Phys. Rev. Lett.*, **87**, 068301 (2001).
6. V. Kochergin, *Omnidirectional Optical Filters*, Kluwer Academic, Boston (2003).
7. V. Kovalev, G. Polisski, J. Diener, H. Heckler, N. Künzner, V.Y. Timoshenko, F. Koch, *Appl. Phys. Lett.*, **78**, 916 (2001).
8. V. Kochergin, M. Christophersen, P.R. Swinehart, *Proc. SPIE*, **5554**, 223 (2004).
9. G. Kaltsas, A.G. Nassiopoulou, *Sens. Actuators A*, **76**, 133 (1999).
10. C.J. Oton, L. Pancheri, Z. Gaburro, L. Pavesi, C. Baratto, G. Faglia, G. Sberveglieri, *Phys. Status Solidi A*, **197**, 523 (2003).
11. Y. Huang, X. Duan, Y. Cui, C.M. Lieber, *Nano Lett.*, **2**, 101 (2002).
12. S. Nakamura, M.R. Krames, *Proc. IEEE*, **101**, 2211 (2013).
13. S.C. Jain, M. Willander, J. Narayan, R.V. Overstraeten, *J. Appl. Phys.*, **87**, 965 (2000).
14. H. Shibata, Y. Waseda, H. Ohta, K. Kiyomi, K. Shimoyama, K. Fujito, H. Nagaoka, Y. Kagamitani, R. Simura, T. Fukuda, *Mater. Trans.*, **48**, 2782 (2007).
15. T. Palacios, A. Chakraborty, S. Rajan, C. Poblenz, S. Keller, S.P. DenBaars, J.S. Speck, U.K. Mishra, *IEEE Electron Device Lett.*, **26**, 781 (2005).

16. M. Leszczynski, H. Teisseyre, T. Suski, I. Grzegory, M. Bockowski, J. Jun, S. Porowski, K. Pakula, J.M. Baranowski, C.T. Foxon, T.S. Cheng, *Appl. Phys. Lett.*, **69**, 73 (1996).
17. R. Dahal, B. Pantha, J. Li, J.Y. Lin, H.X. Jiang, *Appl. Phys. Lett.*, **94**, 063505 (2009).
18. C.J. Neufeld, N.G. Toledo, S.C. Cruz, M. Iza, S.P. DenBaars, U.K. Mishra, *Appl. Phys. Lett.*, **93**, 143502 (2008).
19. S. Strite, H. Morkoç, *J. Vac. Sci. Technol. B*, **10**, 1237 (1992).
20. M. Mynbaeva, N. Bazhenov, K. Mynbaev, V. Evstropov, S.E. Sadow, Y. Koshka, Y. Melnik, *Phys. Status Solidi B*, **228**, 589 (2001).
21. M. Mynbaeva, A. Titkov, A. Kryganovskii, V. Ratnikov, K. Mynbaev, H. Huhtinen, R. Laiho, V. Dmitriev, *Appl. Phys. Lett.*, **76**, 1113 (2000).
22. X. Li, Y.W. Kim, P.W. Bohn, I. Adesida, *Appl. Phys. Lett.*, **80**, 980 (2002).
23. A.P. Vajpeyi, S.J. Chua, S. Tripathy, E.A. Fitzgerald, W. Liu, P. Chen, L.S. Wang, *Electrochem. Solid-State Lett.*, **8**, G85 (2005).
24. M. Ohkubo, *J. Cryst. Growth*, **189-190**, 734 (1998).
25. D.J. Díaz, T.L. Williamson, I. Adesida, P.W. Bohn, R.J. Molnar, *J. Appl. Phys.*, **94**, 7526 (2003).
26. C. Youtsey, I. Adesida, G. Bulman, *Appl. Phys. Lett.*, **71**, 2151 (1997).
27. M. Ainorkhilah, A. Naser Mahmoud, Y. Yuhamdan, F.K. Yam, L.S. Chuah, R.A. Husnen, H. Zainuriah, *Int. J. Electrochem. Sci.*, **8**, 5801 (2013).
28. C.B. Soh, H. Hartono, S.Y. Chow, S.J. Chua, E.A. Fitzgerald, *Appl. Phys. Lett.*, **90**, 053112 (2007).
29. Y. Zhang, B. Leung, J. Han, *Appl. Phys. Lett.*, **100**, 181908 (2012).
30. A. Ramizy, Z. Hassan, K. Omar, *Sens. Actuators B*, **155**, 699 (2011).
31. F.K. Yam, Z. Hassan, *Appl. Surf. Sci.*, **253**, 9525 (2007).
32. J.J. Wierer, A. David, M.M. Megens, *Nat. Photon.*, **3**, 163 (2009).
33. J.C. Vial, A. Bsiesy, F. Gaspard, R. Herino, M. Ligeon, F. Müller, R. Romestain, R.M. Macfarlane, *Phys. Rev. B*, **45**, 14171 (1992).
34. J.M. Hwang, W.H. Hung, H.L. Hwang, *IEEE Photon. Technol. Lett.*, **20**, 608 (2008).
35. R. Wang, D. Liu, Z. Zuo, Q. Yu, Z. Feng, X. Xu, *AIP Adv.*, **2**, 012109 (2012).
36. K. Kim, J. Choi, T.S. Bae, M. Jung, D.H. Woo, *Jpn. J. Appl. Phys.*, **46**, 6682 (2007).
37. S.W. Ryu, J. Park, J.K. Oh, D.H. Long, K.W. Kwon, Y.H. Kim, J.K. Lee, J.H. Kim, *Adv. Funct. Mater.*, **19**, 1650 (2009).
38. C.Y. Cho, S.E. Kang, K.S. Kim, S.J. Lee, Y.S. Choi, S.H. Han, G.Y. Jung, S.J. Park, *Appl. Phys. Lett.*, **96**, 181110 (2010).
39. S. Chhajed, W. Lee, J. Cho, E.F. Schubert, J.K. Kin, *Appl. Phys. Lett.*, **98**, 071102 (2011).
40. X. Fu, B. Zhang, X. Kang, J. Deng, C. Xiong, T. Dai, X. Jiang, T. Yu, Z. Chen, G.Y. Zhang, *Opt. Express*, **19**, A1104 (2011).
41. J.J. Carvajal, J.C. Rojo, *Cryst. Growth Des.*, **9**, 320 (2009).
42. J.J. Carvajal, O.V. Bilousov, D. Drouin, M. Aguiló, F. Díaz, J.C. Rojo, *Microsc. Microanal.*, **18**, 905 (2012).
43. O.V. Bilousov, H. Geaney, J.J. Carvajal, V.Z. Zubialevich, P.J. Parbrook, A. Giguère, D. Drouin, F. Díaz, M. Aguiló, C. O'Dwyer, *Appl. Phys. Lett.*, **103**, 112103 (2013).

44. O.V. Bilousov, J.J. Carvajal, A. Vilalta-Clemente, P. Ruterana, F. Díaz, M. Aguiló, C. O'Dwyer, *Chem. Mater.*, **26**, 1243 (2014).
45. M.M. Sung, C.Kim, S.H. Yoo, C.G. Kim, Y. Kim, *Chem. Vap. Deposition*, **8**, 50 (2002).
46. O.V. Bilousov, J.J. Carvajal, D. Drouin, X. Mateos, F. Díaz, M. Aguiló, C. O'Dwyer, *ACS Appl. Mater. Interfaces*, **4**, 6927 (2012).
47. J.H. Choi, A. Zoukarniev, S.I. Kim, C.W. Baik, M.H. Yang, S.S. Park, H. Suh, U.J. Kim, H.B. Son, J.S. Lee, M. Kim, J.M. Kim, K. Kim, *Nat. Photon.*, **5**, 763 (2011).
48. O.V. Bilousov, J.J. Carvajal, J. Mena, O. Martínez, J. Jiménez, H. Geaney, F. Díaz, M. Aguiló, C. O'Dwyer, *CrystEngComm*, **16**, 10255 (2014).
49. A.E. Wickenden, D.D. Koleske, R.L. Henry, R.J. Gorman, J.C. Culbertson, M.E. Twigg, *J. Electron. Mater.*, **28**, 301 (1999).
50. O.V. Bilousov, J.J. Carvajal, H. Geaney, V.Z. Zubialevich, P.J. Parbrook, O. Martínez, J. Jiménez, F. Díaz, M. Aguiló, C. O'Dwyer, *ACS Appl. Mater. Interfaces*, **6**, 17954 (2014).
51. J.R. Kim, H. Oh, H.M. So, J. Kim, J.J. Kim, *Physica E*, **18**, 225 (2003).
52. G. Cheng, A. Kolmakov, Y. Zhang, O. Moskovits, R. Munden, M.A. Reed, G. Wang, D. Moses, J. Zhang, *Appl. Phys. Lett.*, **83**